Weierstraß-Institut
für Angewandte Analysis und Stochastik
Leibniz-Institut im Forschungsverbund Berlin e. V.

Preprint ISSN 0946 – 8633

Stabilizing poor mass conservation in incompressible flow problems with large irrotational forcing and application to thermal convection

Keith J. Galvin[1], Alexander Linke[2], Leo G. Rebholz[1], Nicholas E. Wilson[1]

submitted: December 20, 2011

[1] Clemson University
Department of Mathematical Sciences
Clemson 29634
U.S.A.
Email: kjgalvi@clemson.edu
rebholz@clemson.edu
newilso@clemson.edu

[2] Weierstrass Institute
Mohrenstr. 39
10117 Berlin
Germany
E-Mail: alexander.linke@wias-berlin.de

No. 1671
Berlin 2011

2010 *Mathematics Subject Classification.* 76D05, 76M10.

Key words and phrases. Mixed finite elements, incompressible Navier-Stokes equations, poor mass conservation, grad-div stabilization, natural convection, Scott-Vogelius element.

This work was partially supported by NSF grants DMS-1016182, DMS-0914478 and DMS1112593.

Edited by
Weierstraß-Institut für Angewandte Analysis und Stochastik (WIAS)
Leibniz-Institut im Forschungsverbund Berlin e. V.
Mohrenstraße 39
10117 Berlin
Germany

Fax: +49 30 2044975
E-Mail: preprint@wias-berlin.de
World Wide Web: http://www.wias-berlin.de/

Abstract

We consider the problem of poor mass conservation in mixed finite element algorithms for flow problems with large rotation-free forcing in the momentum equation. We provide analysis that suggests for such problems, obtaining accurate solutions necessitates either the use of pointwise divergence-free finite elements (such as Scott-Vogelius), or heavy grad-div stabilization of weakly divergence-free elements. The theory is demonstrated in numerical experiments for a benchmark natural convection problem, where large irrotational forcing occurs with high Rayleigh numbers.

1 Introduction

In recent years, mixed finite element methods for the incompressible Stokes and Navier-Stokes equations (NSE) have seen great success in numerical mathematics [4, 11, 21, 9]. In part, this is due to their elegant and compact theory, but also because they deliver rather simple recipes for the construction of convergent numerical schemes with easily predictable convergence rates and other distinctive properties. The great flexibility of mixed finite elements is mainly indebted to the introduction of a space of discretely divergence-free functions circumventing the problematic construction of a divergence-free basis. There is a price to pay for this flexibility, however, since discretely divergence-free functions are in most cases not divergence-free; these discrete schemes lose two - in fact equivalent - fundamental properties of the original continuous problem (assuming homogeneous Dirichlet boundary conditions): 1) the orthogonality of discretely divergence-free functions and rotation-free functions in the L^2-scalar product, and 2) a change of the forcing $\mathbf{f} \rightarrow \mathbf{f} + \nabla\psi$ changes the solution $(\mathbf{u}, p) \rightarrow (\mathbf{u}, p + \psi)$, which leaves the velocity solution invariant. The consequences of this are well-known [11, 21], and for nearly all mixed finite element methods, rather simple flow problems with rotation-free right hand sides can be constructed such that approximate discrete solutions suffer from dramatically large divergence errors which are visible by large spurious oscillations in the discrete velocities [18, 14, 2, 10]. This observation has led to the introduction of stabilization operators augmenting the pure mixed finite element formulation, e.g., the grad-div stabilization and similar methods [18, 21, 19].

But despite this, it has appeared to be quite difficult to find simple, non-academic, physically-relevant flow problems where poor mass conservation is the main difficulty in accurate velocity field prediction(in the eyeball or H^1 error sense). Although the theoretical need for stabilizing poor mass conservation in Stokes and NSE computations is obvious, techniques like grad-div stabilization are often neglected in practice. This may be explained by the fact that it often does not 'improve' the solution (in the eyeball norm), and additionally, grad-div stabilization can make the iterative solution of the underlying linear systems more difficult [18].

It is well known, however, that poor mass conservation will cause error in problems where velocity is coupled to transport [16, 6], but the difficulty here is generally not with the accuracy of the velocity field prediction (again, in the eyeball or H^1 error sense). It is also known that in problems with complicated

pressures (e.g. Bernoulli pressure in rotational form NSE or related models), poor discrete mass conservation does create numerical problems, and stabilization of grad-div type can dramatically improve the solution [13, 17]. Here, it is revealed that the coupling of poor mass conservation and a large complicated pressure cause numerical instability, however in practice, an alternative 'fix' would be to use the convective formulation instead.

The purpose of this paper is to communicate that in flow problems where the forcing of the momentum equation has a large rotation-free part, poor mass conservation in Stokes and NSE simulations can be a serious problem that is not sufficiently accounted for with standard techniques such as local mass conservation and grad-div stabilization with $\gamma \sim O(1)$ parameter (recall grad-div stabilization is done by adding $0 = -\gamma\nabla(\nabla \cdot \mathbf{u})$ to the momentum equation, then discretizing, which yields the term $\gamma(\nabla \cdot \mathbf{u}_h, \nabla \cdot \mathbf{v}_h)$ in a finite element method) . We provide analysis in Section 2 that suggests in these types of problems, the size of the grad-div parameter may need to be significantly larger than $O(1)$, and depends on both the size of the forcing and the ratio of the rotation-free part of the forcing to the divergence-free part. In Section 3, we test the theory on the physically-relevant application problem of natural convection with large Rayleigh number. This problem has a large rotation-free forcing of the momentum equation caused by buoyancy, and our numerical tests show that to get accurate answers (without excessively refining the mesh - which is of course another way to improve discrete mass conservation), heavy grad-div stabilization is necessary if standard elements such as $((P_2)^d, P_1)$ Taylor-Hood or $((P_2)^d, P_0)$ mixed finite elements are used to approximate velocity and pressure. However, accurate answers are also obtained with $((P_2)^d, P_1^{disc})$ Scott-Vogelius elements, which is consistent with our theory since these elements provide pointwise mass conservation in their velocity solutions and thus the velocity error decouples from rotation-free effects in the momentum equation.

2 Decomposition of momentum forcing and the effect of the irrotational part on velocity error

In this section, we provide an analysis which shows that the standard parameter choice for the grad-div stabilization parameter $\gamma \sim \mathcal{O}(1)$, presented, e.g., in [18, 21], is not always adequate, and can be far from optimal. This standard choice is justified in a paradigmatic way in the excellent article [18], by deriving an optimal a-priori estimate for a Stokes model problem with homogeneous Dirichlet boundary conditions: find $(\mathbf{u}, p) \in H_0^1(\Omega)^d \times L_0^2(\Omega)$ in a Lipschitz domain Ω in two or three space dimensions such that, for all $(\mathbf{v}, q) \in H_0^1(\Omega)^d \times L_0^2(\Omega)$ hold

$$\begin{aligned} \nu(\nabla\mathbf{u}, \nabla\mathbf{v}) - (p, \nabla \cdot \mathbf{v}) &= (\mathbf{f}, \mathbf{v}), \\ (q, \nabla \cdot \mathbf{u}) &= 0, \end{aligned} \tag{1}$$

assuming $\mathbf{f} \in L^2(\Omega)^d$. This model problem is approximated by the conforming LBB-stable mixed finite-element P1isoP2/P0 with grad-div stabilization parameter $\gamma = 1$. For this stabilized discretization of (1), the authors of [18] derive rigorously for this stabilized discretization in (4.13) of [18] the estimate

$$\nu^{\frac{1}{2}} \|\nabla\mathbf{u} - \nabla\mathbf{u}_h\|_0 + \|\nabla \cdot (\mathbf{u} - \mathbf{u}_h)\|_0 + \|p - p_h\| \leq Ch\left(\|\mathbf{u}\|_2 + \|p\|_1\right).$$

The point that we want to make in this article is the role of the pressure in this estimate. Suppose that the right hand side $\mathbf{f}$ of the above model problem would be rotation-free, i.e., $\mathbf{f} = \nabla\varphi \in L_0^2(\Omega)$ for

some scalar potential $\varphi \in H^1(\Omega)$. Then, the solution of the above model problem is $(\mathbf{u}, p) = (0, \varphi)$. With such a simple velocity solution, one might expect a stable and convergent discretization of the Stokes equation to find an accurate approximation, but if mixed finite elements are used, only very special element choices which provide pointwise divergence free velocity solution (such as Scott-Vogelius elements) will find a discrete velocity solution $\mathbf{u}_h = \mathbf{0}$. But for mixed finite elements whose discrete solutions are only discretely divergence-free, the approximation error of the discrete solution $\mathbf{u}_h$ of the above model problem will scale in the H_1-norm with $\|\nabla\varphi\|_0$. In this case, the grad-div stabilization parameter $\gamma = 1$ only helps to mitigate the negative effect of a small parameter ν. This mitigation can be seen in the estimate (4.12) of [18] for the P1isoP2/P0 element without grad-div stabilization

$$\nu^{\frac{1}{2}} \|\nabla\mathbf{u} - \nabla\mathbf{u}_h\|_0 + \|p - p_h\| \leq Ch \left(\|\mathbf{u}\|_2 + \nu^{-\frac{1}{2}} \|p\|_1 \right).$$

This discussion leads to (at least) two important questions: 1) How can we bridge the gap between the perfect results for the Scott-Vogelius element and other mixed finite elements, and 2) How relevant is the above example with a rotation-free right hand side $\mathbf{f} = \varphi$ in practice? For the first question, we answer that indeed there is a possibility to bridge the gap: using a very large stabilization γ will enforce the discrete velocity solution be nearly zero. We want to show in this article that a choice of the stabilization parameter like $\gamma \gg 1$ can be a good choice, whenever the rotation-free part of the right hand side $\mathbf{f}$ is stronger than the divergence-free part of $\mathbf{f}$. In other words, we argue that for an adequate choice of the grad-div stabilization we have to consider the Helmholtz-Hodge decomposition of $\mathbf{f}$. For the second question, we will present a simple, but physically relevant example: natural convection in a differentially heated cavity, which shows that in practice grad-div stabilization parameters of $\gamma \gg 1$ can be sometimes possible and necessary at the same time. Last but not least, we want to remark that our analysis for the choice of the grad-div stabilization parameter is not so much based on an a-priori error estimate, but on a-priori stability estimates, where the importance of the Helmholtz decomposition for the choice of γ becomes much clearer.

2.1 Helmholtz-Hodge decomposition

In order to make plausible our arguments, we introduce the orthogonal Helmholtz-Hodge decomposition of a vector field $\mathbf{f} \in L^2(\Omega)^d$. This decomposition provides

$$\mathbf{f} = \nabla\varphi + \mathbf{w},$$

where $(\nabla\varphi, \mathbf{w}) = 0$, φ is the only solution $\varphi \in H^1(\Omega)/\mathbb{R}$ of

$$(\nabla\varphi, \nabla\mu) = (\mathbf{f}, \nabla\mu)$$

for all $\mu \in H^1(\Omega)/\mathbb{R}$, and $\mathbf{w} \in L^2(\Omega)^d$ satisfying $\nabla \cdot \mathbf{w} = 0$. The vector $\mathbf{w}$ is called the divergence-free part of $\mathbf{f}$, and $\nabla\varphi$ is called the rotation-free part of $\mathbf{f}$. Using this decomposition, we obtain the following a-priori stability estimate for the velocity,

$$\|\nabla\mathbf{u}\|_0 \leq \frac{C_F}{\nu} \|\mathbf{w}\|_0,$$

where C_F denotes the Poincaré-Friedrichs constant. We remark that only the L^2-norm $\|\mathbf{w}\|_0$ of the divergence-free part of $\mathbf{f}$ enters the velocity stability estimate, since rotation-free functions $\nabla\varphi$ are

$L^2(\Omega)^d$-orthogonal to divergence-free functions. In fact, the velocity solution is not affected at all by the rotation free part of **f**. Denoting the solution of the above Stokes problem for a given $\mathbf{f} \in L^2(\Omega)^d$ by $(\mathbf{u}_0, p_0)$, it is easy to see that the corresponding Stokes solution $(\mathbf{u}_\varphi, p_\varphi)$ for the right hand side $\mathbf{f} + \nabla\psi$ with $\psi \in H^1(\Omega)/\mathbb{R}$ will be given by $(\mathbf{u}_\psi, p_\psi) = (\mathbf{u}_0, p_0 + \psi)$.

2.2 The discrete setting

For the finite element discretization, we use LBB-stable mixed finite elements with grad-div stabilization in order to mitigate problems with poor mass conservation. We choose pairs of conforming finite element spaces $V_h \subset H_0^1(\Omega)^d$ and $Q_h \subset L_0^2(\Omega)$ that satisfy the LBB condition (see, e.g. [3, 12]). The stabilized finite element discretization reads: For fixed $\gamma \geq 0$, find $(\mathbf{u}_h, p_h) \in V_h \times Q_h$ such that for all $(\mathbf{v}_h, q_h) \in V_h \times Q_h$,

$$\begin{aligned} \nu(\nabla\mathbf{u}_h, \nabla\mathbf{v}_h) + \gamma(\nabla\cdot\mathbf{u}_h, \nabla\cdot\mathbf{v}_h) - (p_h, \nabla\cdot\mathbf{v}_h) &= (\mathbf{f}, \mathbf{v}_h), \\ (q_h, \nabla\cdot\mathbf{u}_h) &= 0. \end{aligned} \tag{2}$$

For the stabilization parameter γ we can choose any non-negative real value, and finding good choices for this parameter is the goal of the following analysis. We introduce now the spaces of weakly differentiable divergence-free functions, and discretely divergence-free functions

$$\begin{aligned} V_0 &= \{\mathbf{v} \in H_0^1(\Omega)^d : \nabla\cdot\mathbf{v} = 0\}, \\ V_{0,h} &= \{\mathbf{v}_h \in V_h : (\nabla\cdot\mathbf{v}_h, q_h) = 0 \text{ for all } q_h \in Q_h\}. \end{aligned}$$

In general, $V_{0,h} \not\subset V_0$, i.e., discretely divergence-free functions need not to be divergence-free, except for only a very few element pair choices. The space of divergence-free discretely-divergence-free functions

$$V_{00,h} := V_{0,h} \cap V_0,$$

also becomes important for the numerical approximation of the Stokes problem. Further, we introduce the orthogonal complement of $V_{00,h}$ in $V_{0,h}$ with respect to the scalar product $(\nabla\mathbf{u}, \nabla\mathbf{v})$ via

$$R_h := \{\mathbf{r}_h \in V_{0,h} : (\nabla\mathbf{r}_h, \nabla\mathbf{v}_h) = 0 \quad \text{for all} \quad \mathbf{v}_h \in V_{00,h}\}.$$

Note that $\|\nabla\cdot\mathbf{s}_h\|_0$ for $\mathbf{s} \in R_h$ defines a norm on the space R_h. The reason for this is that R_h is an orthogonal complement to $V_{00,h}$ in $V_{0,h}$. Therefore, the only divergence-free function in R_h is the velocity $\mathbf{0}$. Now, in the finite dimensional space R_h there exists

$$M_h := \max_{\mathbf{v}_h \in R_h, \|\nabla\mathbf{v}_h\|_0 = 1} \frac{1}{\|\nabla\cdot\mathbf{v}_h\|_0},$$

and for all $\mathbf{0} \neq \mathbf{s} \in R_h$ holds

$$\|\nabla\mathbf{s}_h\|_0 = \frac{\|\nabla\mathbf{s}_h\|_0}{\|\nabla\cdot\mathbf{s}\|_0}\|\nabla\cdot\mathbf{s}\|_0 = \frac{1}{\left\|\nabla\cdot\frac{\mathbf{s}}{\|\nabla\mathbf{s}\|_0}\right\|_0}\|\nabla\cdot\mathbf{s}\|_0 \leq M_h\|\nabla\cdot\mathbf{s}_h\|_0. \tag{3}$$

The constant M_h depends on the mesh, and the chosen mixed finite element. We remark that for a conforming LBB-stable mixed finite element whose velocity converges in the H^1-norm with order k, the constant M_h scales with order h^{-k}, in general. This can be derived easily by the following argument: imagine that the space $V_{00,h}$ contains only the velocity $\mathbf{0}$. Then, any smooth divergence-free velocity $\mathbf{u}$ can be approximated by non-divergence-free velocities $\mathbf{v}_h \in R_h$ with optimal order h^k in the H^1-norm. Then, also $\nabla\cdot\mathbf{u}$ converges with order h^k to zero, and M_h must grow with order h^{-k}. Finally, we note that a sharper estimate of the size of M_h in (3) may be possible.

2.3 Stabilizing for poor discrete mass conservation based on the forcing

We begin our analysis by decomposing the discrete solution $\mathbf{u}_h$ and the test functions $\mathbf{v}_h$ by

$$\begin{aligned}\mathbf{u}_h &= \mathbf{u}_{00,h} + \mathbf{r}_h,\\ \mathbf{v}_h &= \mathbf{v}_{00,h} + \mathbf{s}_h\end{aligned}$$

with $\mathbf{u}_{00,h}$, $\mathbf{v}_{00,h} \in V_{00,h}$ and $\mathbf{r}_h, \mathbf{s}_h \in R_h$. From Galerkin orthogonality and the orthogonality of the decomposition, we obtain from (2) the following two equations for $\mathbf{u}_{00,h}$ and $\mathbf{r}_h$

$$\begin{aligned}(\nabla(\mathbf{u}_{00,h} - \mathbf{u}), \nabla\mathbf{v}_{00,h}) &= 0,\\ \nu(\nabla\mathbf{r}_h, \nabla\mathbf{s}_h) + \gamma(\nabla\cdot\mathbf{r}_h, \nabla\cdot\mathbf{s}_h) &= (\mathbf{f}, \mathbf{s}_h)\end{aligned} \tag{4}$$

for all $\mathbf{v}_{00,h} \in V_{00,h}$ and $\mathbf{s}_h \in R_h$. Therefore, $\mathbf{u}_{00,h}$ is the projection of $\mathbf{u}$ into the space $V_{00,h}$ with respect to the scalar product $(\nabla\mathbf{u}, \nabla\mathbf{v})$. We remark that in some cases, already the approximation $\mathbf{u}_{00,h}$ of $\mathbf{u}$ does converge with optimal convergence order, for example if Scott-Vogelius elements are used on an appropriate mesh.

For $\mathbf{u}_{00,h}$ with general mixed element choice, we obtain the same stability estimate as in the continuous case, since it is the H^1-projection of $\mathbf{u}$ onto $V_{00,h}$, i.e.

$$\|\nabla\mathbf{u}_{00,h}\|_0 \leq \|\nabla\mathbf{u}\|_0 \leq \frac{C_F}{\nu}\|\mathbf{w}\|_0 .$$

We now investigate in detail the non-divergence-free part of the discrete velocity solution, $\mathbf{r}_h \in R_h$. Using Galerkin orthogonality in (4) for $\mathbf{r}_h$ we obtain

$$\nu(\nabla(\mathbf{r}_h - \mathbf{u}), \nabla\mathbf{s}_h) + \gamma(\nabla\cdot\mathbf{r}_h, \nabla\cdot\mathbf{s}_h) = -(p, \nabla\cdot\mathbf{s}_h)$$

for all $\mathbf{s}_h \in R_h$. Obviously, we would obtain the best possible approximation for $\mathbf{r}_h$, if

$$\gamma(\nabla\cdot\mathbf{r}_h, \nabla\cdot\mathbf{s}_h) = -(p, \nabla\cdot\mathbf{s}_h)$$

for all $\mathbf{s}_h \in R_h$, since then $\mathbf{r}_h$ would be the H^1-projection of $\mathbf{u}$ onto R_h. But we want that this relation holds at least approximately, and we estimate possible values for γ. We remark since $(\nabla\cdot\mathbf{r}_h, \nabla\cdot\mathbf{s}_h)$ is a scalar product on R_h, for a fixed $\gamma > 0$, exactly one $\mathbf{r}_h \in R_h$ solves

$$\gamma(\nabla\cdot\mathbf{r}_h, \nabla\cdot\mathbf{s}_h) = -(p, \nabla\cdot\mathbf{s}_h) \quad \text{for all} \quad \mathbf{s}_h \in R_h.$$

From (4) we derive the estimate

$$\gamma\|\nabla\cdot\mathbf{r}_h\|_0^2 \leq C_F\|\mathbf{f}\|_0\|\nabla\mathbf{r}_h\|_0 ,$$

which combined with (3), delivers

$$\|\nabla\cdot\mathbf{r}_h\|_0 \leq \frac{C_F M_h}{\gamma}\|\mathbf{f}\|_0 \tag{5}$$

with the mesh-dependent constant M_h. Further, if R_h is nonempty, the relation

$$\nu(\nabla(\mathbf{r}_h - \mathbf{u}), \nabla\mathbf{s}_h) \approx 0 \quad \text{for all} \quad \mathbf{s}_h \in R_h$$

can only hold when the norms of $\|\nabla \mathbf{u}\|_0$ and $\|\nabla \mathbf{r}_h\|_0$ are comparable. Therefore, the relation $\nabla \mathbf{r}_h \sim \nabla \mathbf{u}$ requires $\|\nabla \cdot \mathbf{r}_h\|_0 \lesssim \|\nabla \mathbf{u}\|_0$ to hold. This is approximately fulfilled if

$$\frac{C_F M_h}{\gamma} \|\mathbf{f}\|_0 \lesssim \frac{C_F}{\nu} \|\mathbf{w}\|_0 \qquad \Leftrightarrow \qquad \gamma \gtrsim M_h \nu \frac{\|\mathbf{f}\|_0}{\|\mathbf{w}\|_0} = M_h \nu \frac{\|\mathbf{w}\|_0 + \|\nabla \varphi\|_0}{\|\mathbf{w}\|_0}. \tag{6}$$

From (5), we learn that a reasonable choice of γ should scale proportionally to $\|\mathbf{f}\|_0$, and from (6) we see that the choice of γ depends also on the ratio

$$\frac{\|\mathbf{w}\|_0 + \|\nabla \varphi\|_0}{\|\mathbf{w}\|_0}.$$

We remark that for finer and finer mesh sizes h, the estimate (5) becomes more and more pessimistic, and loses its value for a sensible determination of γ. The important point of the above estimates is that we can predict that a good γ should scale with $\frac{\|\mathbf{w}\|_0 + \|\nabla \varphi\|_0}{\|\mathbf{w}\|_0}$.

A last remark is that for very large stabilization parameters γ the above derivations tell us that then $\mathbf{r}_h \in R_h$ is determined by

$$(\nabla \cdot \mathbf{r}_h, \nabla \cdot \mathbf{s}_h) = \frac{1}{\gamma}(\mathbf{f}, \mathbf{s}_h)$$

for all $\mathbf{s}_h \in R_h$, since $\nu(\nabla \mathbf{r}_h, \nabla \mathbf{s}_h)$ converges to zero for a fixed $\mathbf{s}_h \in R_h$.

3 The natural convection problem in a differentially heated cavity

We investigate natural convection in a differentially heated cavity, which can be modeled by the following incompressible Navier-Stokes-Boussinesq system in $\Omega = (0,1)^2$:

$$\frac{1}{\mathrm{Pr}} \left(\mathbf{u}_t + (\mathbf{u} \cdot \nabla) \mathbf{u} \right) - \Delta \mathbf{u} + \nabla p = \mathrm{Ra} T \mathbf{e}_y, \tag{7}$$

$$\nabla \cdot \mathbf{u} = 0, \tag{8}$$

$$T_t - \Delta T + \mathbf{u} \cdot \nabla T = 0, \tag{9}$$

with boundary conditions corresponding to internal flow with the top and bottom insulated, and heating/cooling applied to the left and right side:

$$T = 1, \ \ \mathbf{x} \in \Gamma_1 := \{0\} \times (0,1), \tag{10}$$

$$T = 0, \ \ \mathbf{x} \in \Gamma_2 := \{1\} \times (0,1), \tag{11}$$

$$\nabla T \cdot \mathbf{n} = 0, \ \ \mathbf{x} \in \Gamma 3 := (0,1) \times \{0,1\}. \tag{12}$$

$$\mathbf{u} = \mathbf{0}, \ \ \mathbf{x} \in \partial\Omega = \Gamma_1 \cup \Gamma_2 \cup \Gamma_3. \tag{13}$$

A diagram of the domain and boundary conditions is shown in Figure 1.

This flow is driven by buoyancy caused by thermal expansion. Using the so-called Boussinesq approximation for small temperature differences, this flow is modeled with the incompressible NSE to account for the thermal expansion of the fluid in the momentum equations via the force field $\mathrm{Ra}T\mathbf{e}_y$[1, 7, 8], where the (non-dimensional) Rayleigh number Ra measures the relative strength of buoyancy with respect to thermal and momentum diffusivities. This problem admits stable steady solutions up to very large Rayleigh numbers, as high as $\mathrm{Ra} = 10^7$ [1, 7], and is interesting for this study because such large Ra will cause a large forcing in the momentum equation. Moreover, since only the divergence-free part of $\mathrm{Ra}T\mathbf{e}_y$ is physically relevant for the fluid motion, the remaining rotation-free part of the force is completely absorbed by the pressure gradient. Thus, this large rotation-free part of the force field $\mathrm{Ra}T\mathbf{e}_y$ makes this fit in the class of problems we describe in the previous sections.

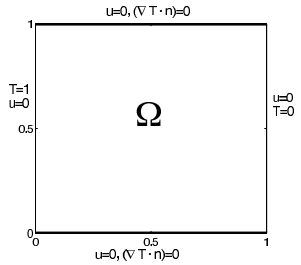

Figure 1: The domain and boundary conditions for the natural convection problem.

We test several mixed finite element methods, and with varying grad-div stabilization parameters γ, for the natural convection problem and compare their accuracy. Of particular importance for this comparison is the use of the Scott-Vogelius (SV) elements, which is one of the rare mixed finite element methods whose space of discretely divergence-free functions contains only divergence-free functions. Therefore, the SV element never suffers from the problem of poor mass conservation. We will compare this element with classical mixed finite elements like the Taylor-Hood (TH) element, and will show how the grad-div stabilization improves the numerical results, and moreover, that for this problem, large γ give better results (which agrees with our theory).

We approximate solutions to the system (7)-(9) using the finite element method. Some notation is necessary to define the numerical algorithm, and we begin with the function spaces

$$\begin{aligned} X :=& \{\mathbf{v} \in H^1(\Omega)^d,\ \mathbf{v} = \mathbf{0} \text{ on } \partial\Omega\}, \\ Q :=& \{q \in L^2(\Omega),\ \int_\Omega q = 0\}, \\ W :=& \{S \in H^1(\Omega),\ S(0,y) = 0 \text{ on } \Gamma_2\}. \\ W^0 :=& \{S \in H^1(\Omega),\ S(0,y) = 0 \text{ on } \Gamma_2 \cup \Gamma_3\}. \end{aligned}$$

For a given regular mesh τ_h, the finite dimensional subspaces $X_h \subset X$, $Q_h \subset Q$, $W_h \subset W$, and $W_h^0 \subset W^0$ will be defined as polynomials on each element of the mesh. We will use four different choices of element triplets (X_h, Q_h, W_h) in our computations, but in all cases temperatures are approximated with continuous element-wise quadratics:

1. Scott-Vogelius (SV): $(X_h, Q_h, W_h) := (\mathbf{P}_2, P_1^{disc}, P_2)$

2. Taylor-Hood (TH) : $(X_h, Q_h, W_h) := (\mathbf{P}_2, P_1, P_2)$

3. P2P0: $(X_h, Q_h, W_h) := (\mathbf{P}_2, P_0, P_2)$

4. P1bubble-P1 (P1B): $(X_h, Q_h, W_h) := (\mathbf{P}_1^{bub}, P_1, P_2)$

While the TH, P2P0 and P1B choices are known to be LBB stable on any regular triangular mesh [3], the LBB stability of SV elements requires the mesh to have a specific macro-element structure, which is satisfied, for example, if the mesh is created as a barycenter refinement of a regular triangular mesh [20]. We consider this a mild mesh restriction, and for a fair comparison of solutions between the element choices, we will use such a barycenter refined mesh for all element choices in our computations, and for the non-SV elements, we will also compute on a non barycenter refined mesh yielding roughly the same number of degrees of freedom.

Taking Ra=10^6, the test problem we consider is known to have a stable steady solution, so we will solve the steady problem directly with the algorithm: Find $(\mathbf{u}_h, p_h, T_h) \in (X_h, Q_h, W_h)$ satisfying $\forall (\mathbf{v}_h, q_h, S_h) \in (X_h, Q_h, W_h^0)$,

$$\begin{aligned}
\frac{1}{Pr}\left(\frac{1}{2}(\mathbf{u}_h \cdot \nabla \mathbf{u}_h, \mathbf{v}_h) - \frac{1}{2}(\mathbf{u}_h \cdot \nabla \mathbf{v}_h, \mathbf{u}_h)\right) - (p_h, \nabla \cdot \mathbf{v}_h) & \\
+\gamma(\nabla \cdot \mathbf{u}_h, \nabla \cdot \mathbf{v}_h) + (\nabla \mathbf{u}_h, \nabla \mathbf{v}_h) &= Ra(T\mathbf{e}_y, \mathbf{v}_h), \qquad (14)\\
(\nabla \cdot \mathbf{u}_h, q_h) &= 0, \qquad (15)\\
\frac{1}{2}(\mathbf{u}_h \cdot \nabla T_h, S_h) - \frac{1}{2}(\mathbf{u}_h \cdot \nabla S_h, T_h) + (\nabla T_h, \nabla S_h) &= 0, \qquad (16)\\
T_h(0, y) &= 1. \qquad (17)
\end{aligned}$$

The skew-symmetrization of the nonlinear terms and grad-div stabilization is used because $\nabla \cdot \mathbf{u}_h \neq 0$ for most of our choices of elements. With SV elements, neither of these is necessary, although their use will not change the solution since the divergence error will be on the order of machine error (in this case one can choose $q_h = \nabla \cdot \mathbf{u}_h$ in (15) and so $\|\nabla \cdot \mathbf{u}_h\| = 0$). However, the use of grad-div stabilization does increase the condition number of the resulting linear systems, and so we set $\gamma = 0$ when using SV elements. We also note that the nonlinearity of the problem is resolved with the standard Newton method.

Recent work in [5, 15] has established a strong connection between finite element solutions of Stokes and Navier-Stokes problems, computed with SV elements, and with grad-div stabilized TH or P2P0 elements. This result essentially states that on a mesh where SV elements are LBB stable and if a unique SV solution exists, solutions found using TH or P2P0 corresponding to chosen grad-div parameter γ, will converge to the SV solution as $\gamma \to 0$ with rate $O(\gamma^{-1})$. This result can be easily extended to (14)-(17), assuming uniqueness conditions on the data similar to those in [7], as follows.

Lemma 3.1. *Suppose τ_h be a barycenter refinement of a regular triangular mesh, and let the problem data be such that the SV solution to* (14)-(17) *is unique. Then as $\gamma \to \infty$,*

$$\begin{aligned}
\|u_h^{TH} - u_h^{SV}\| = O(\gamma^{-1}), \qquad & \|u_h^{P2P0} - u_h^{SV}\| = O(\gamma^{-1})\\
\|(p_h^{TH} - \gamma(\nabla \cdot u_h^{TH})) - p_h^{SV}\| = O(\gamma^{-1}), \qquad & \|(p_h^{P2P0} - \gamma(\nabla \cdot u_h^{P2P0})) - p_h^{SV}\| = O(\gamma^{-1})\\
\|T_h^{TH} - T_h^{SV}\| = O(\gamma^{-1}), \qquad & \|T_h^{P2P0} - T_h^{SV}\| = O(\gamma^{-1}).
\end{aligned} \qquad (18)$$

Proof. The proof of this lemma is an easy extension of the NSE case, proven in [15]. □

Remark 3.1. *This result relies on Scott-Vogelius solutions existing uniquely, which is only true in the case when LBB holds and (it seems) for small data. For general meshes, large grad-div parameters can cause solution inaccuracy, as demonstrated in [5], and there is no guarantee that the divergence-free subspace of X_h has optimal approximation properties.*

3.1 Comparison of solutions for natural convection in air (Pr=0.71)

We now consider solving the natural convection problem that models air flow, and we take $Pr = 0.71$ and $Ra = 10^6$. We first compute a reference solution, using SV and a mesh that provides 36,962 velocity degrees of freedom (dof), 27,360 pressure dof, and 18,481 dof for the temperature. The mesh used, and the velocity streamlines, and temperature and pressure contours for the reference solution are shown in Figure 2. These plots of the solution agree with those found in the literature, e.g. [7].

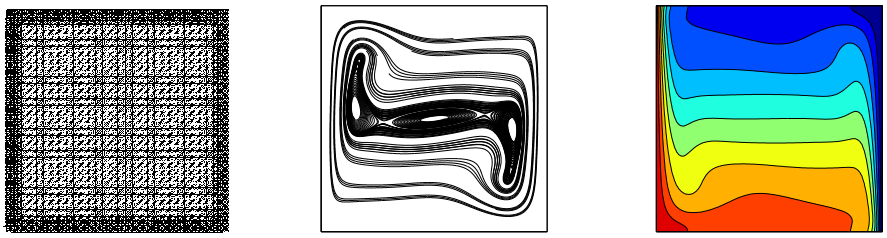

Figure 2: The mesh, velocity streamlines, and temperature contours of the reference solution.

We now approximate solutions on coarser meshes. On fine enough meshes, most element choices can be expected to find similar good answers that enforce mass conservation well, but on coarser meshes where only marginal resolution is possible, large differences in their solutions may be present. Due to the large number of dof necessary to compute approximations to most fluid flow problems, the comparison on the coarser meshes is quite relevant to practical computations, since marginal resolution is often the best one can get.

First, we compute solutions for SV, TH, and P2P0 on the barycenter refined mesh shown in Figure 3, which is created by a 7 x 7 uniform mesh that is refined once around the boundary, then given a barycenter refinement over the entire mesh; this mesh provides 2,538 and 1,269 dof for velocity and temperature, and for pressure, 1,746, 582, and 344 for SV, TH, and P2P0, respectively. Next, we repeat the calculations for TH and P2P0 on a non-barycenter refined mesh (SV is not LBB stable on this mesh) that provides roughly the same number of degrees of freedom: 2,778 and 1,389 dof for velocity and temperature, and 1,998, 666, and 362 pressure dof for SV, TH, and P2P0 respectively. Lastly, we compute with P1B and varying γ, on a finer mesh that provides 6,802, 745, 2,073 dof for velocity, pressure and temperature, respectively.

Results are shown as velocity streamlines and temperature contours in Figures 4-6. The divergence errors are shown in Table 1, and are as expected, with SV providing much better mass conservation than the other methods, and the other methods' mass conservation improving as γ increases. Note that SV does not provide 'exact' mass conservation due to roundoff error, and since the size of $\|\nabla \mathbf{u}\| \approx 10^3$; however, it is still 10 orders of magnitude better than the TH, P2P0 and P1B solutions when $\gamma = 0$ was used.

Figure 4 shows results of computations on the barycenter refined mesh for SV, TH and P2P0 with varying γ. We observe that SV finds a good solution that matches the reference solution, while both TH and P2P0 need heavy grad-div stabilization to find good solutions. With γ small, both TH and P2P0 have poor accuracy in their velocity streamlines, and oscillations in their temperature contours. When $\gamma = 0$, no TH solution was obtained as the Newton iteration failed. Figure 5 shows results of computations on the non-barycenter refined mesh for TH and P2P0 with varying γ. We observe similar results as those on the barycenter refined mesh, in that both TH and P2P0 need heavy grad-div stabilization to find good solutions.

Figure 6 shows the results of the P1B element on a finer, non barycenter refined mesh, with varying γ. Here we observe that with small γ, the velocity streamlines are inaccurate and the temperature contours show slight oscillations and also some deviation from the reference solution. The solution improves as γ increases to 10 and 100, but by $\gamma = 1,000$, the improvement stops as the velocity streamlines and temperature contours become distorted. This suggests that with this low order element, stronger enforcement of mass conservation harms the solution. This is not particularly surprising, since the P1B element has less local degrees of freedom than higher order elements, and therefore cannot absorb 'extra' constraints.

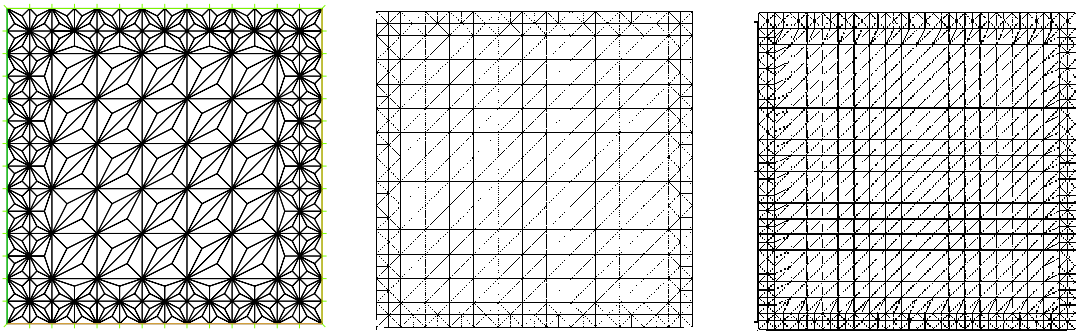

Figure 3: The meshes used in the numerical experiments to compare solutions using different element choices and grad-div parameters. The meshes on the left and middle are used for SV, TH and P2P0, and the mesh on the right is used for P1B.

element	mesh	γ	$\|\nabla \cdot u_h\|$
SV	barycenter	0	1.04953e-7
P2P0	barycenter	0	1399.25
P2P0	barycenter	1	1018.89
P2P0	barycenter	10	(Newton failed)
P2P0	barycenter	100	73.9032
P2P0	barycenter	1k	7.77961
P2P0	barycenter	10k	0.781539
TH	barycenter	0	(Newton failed)
TH	barycenter	1	216.276
TH	barycenter	10	56.3198
TH	barycenter	100	7.51701
TH	barycenter	1,000	0.780873
TH	barycenter	10,000	0.078395
P2P0	coarser non-bary	0	1690.67
P2P0	coarser non-bary	1	1133.34
P2P0	coarser non-bary	10	428.596
P2P0	coarser non-bary	100	60.8438
P2P0	coarser non-bary	1,000	6.29827
P2P0	coarser non-bary	10,000	0.632025
TH	coarser non-bary	0	91.4042
TH	coarser non-bary	1	54.8908
TH	coarser non-bary	10	21.2521
TH	coarser non-bary	100	4.44583
TH	coarser non-bary	1,000	0.550115
TH	coarser non-bary	10,000	0.0569602
(P1b,P1)	finer non-bary	0	290.136
(P1b,P1)	finer non-bary	1	181.024
(P1b,P1)	finer non-bary	10	73.256
(P1b,P1)	finer non-bary	100	40.757
(P1b,P1)	finer non-bary	1,000	25.987
(P1b,P1)	finer non-bary	10,000	8.011

Table 1: Mass conservation of the different solutions for Ra=10^6 and Pr=0.71.

SV

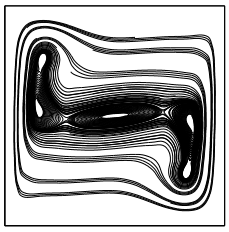

TH ($\gamma = 0$) - Newton Failed

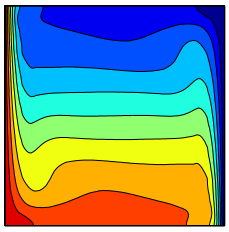

TH ($\gamma = 1$)

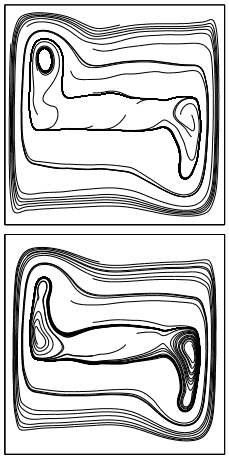

TH ($\gamma = 10$)

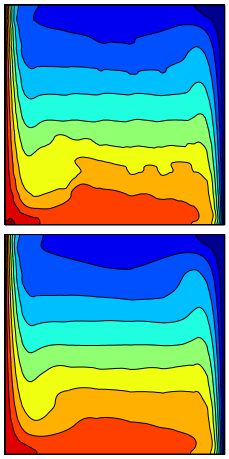

TH ($\gamma = 100$)

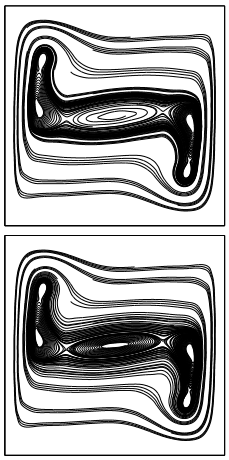

TH ($\gamma = 1,000$)

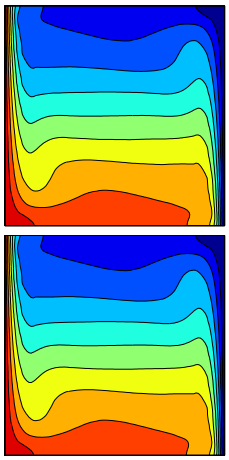

P2P0 ($\gamma = 0$)

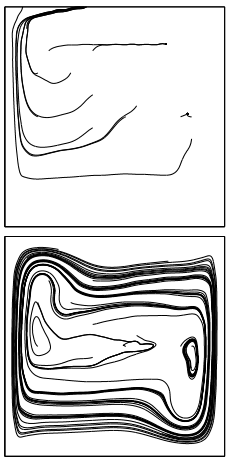

P2P0 ($\gamma = 100$)

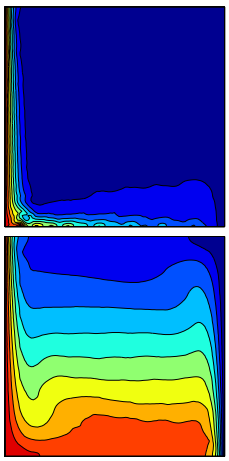

P2P0 ($\gamma = 1,000$)

P2P0 ($\gamma = 10,000$)

TH($\gamma = 0$)

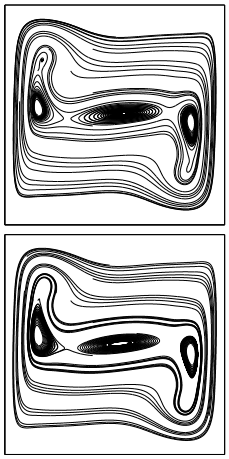

TH ($\gamma = 1$)

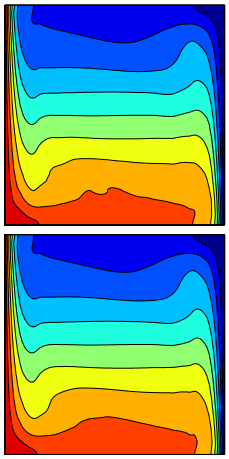

TH ($\gamma = 10$)

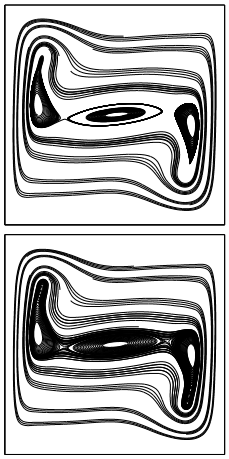

TH ($\gamma = 100$)

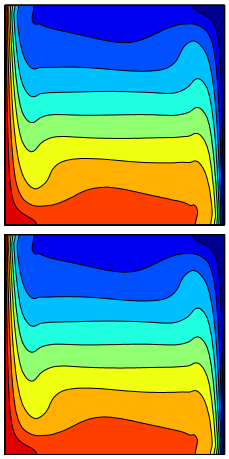

TH ($\gamma = 1,000$)

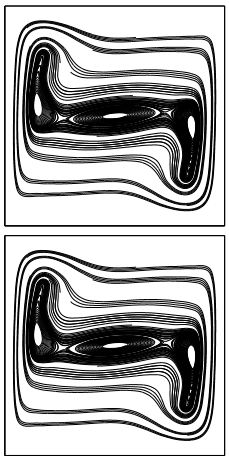

TH ($\gamma = 10,000$)

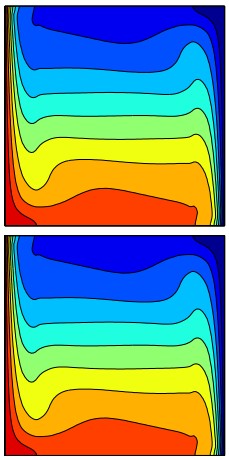

P2P0 ($\gamma = 0$)

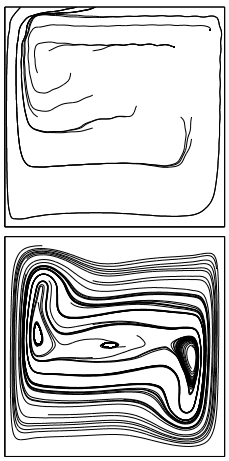

P2P0 ($\gamma = 100$)

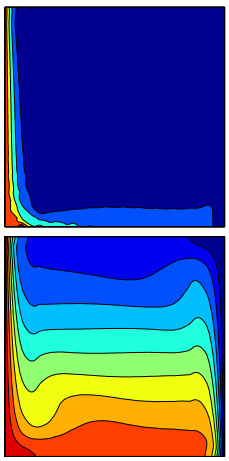

P2P0 ($\gamma = 1,000$)

P2P0 ($\gamma = 10,000$)

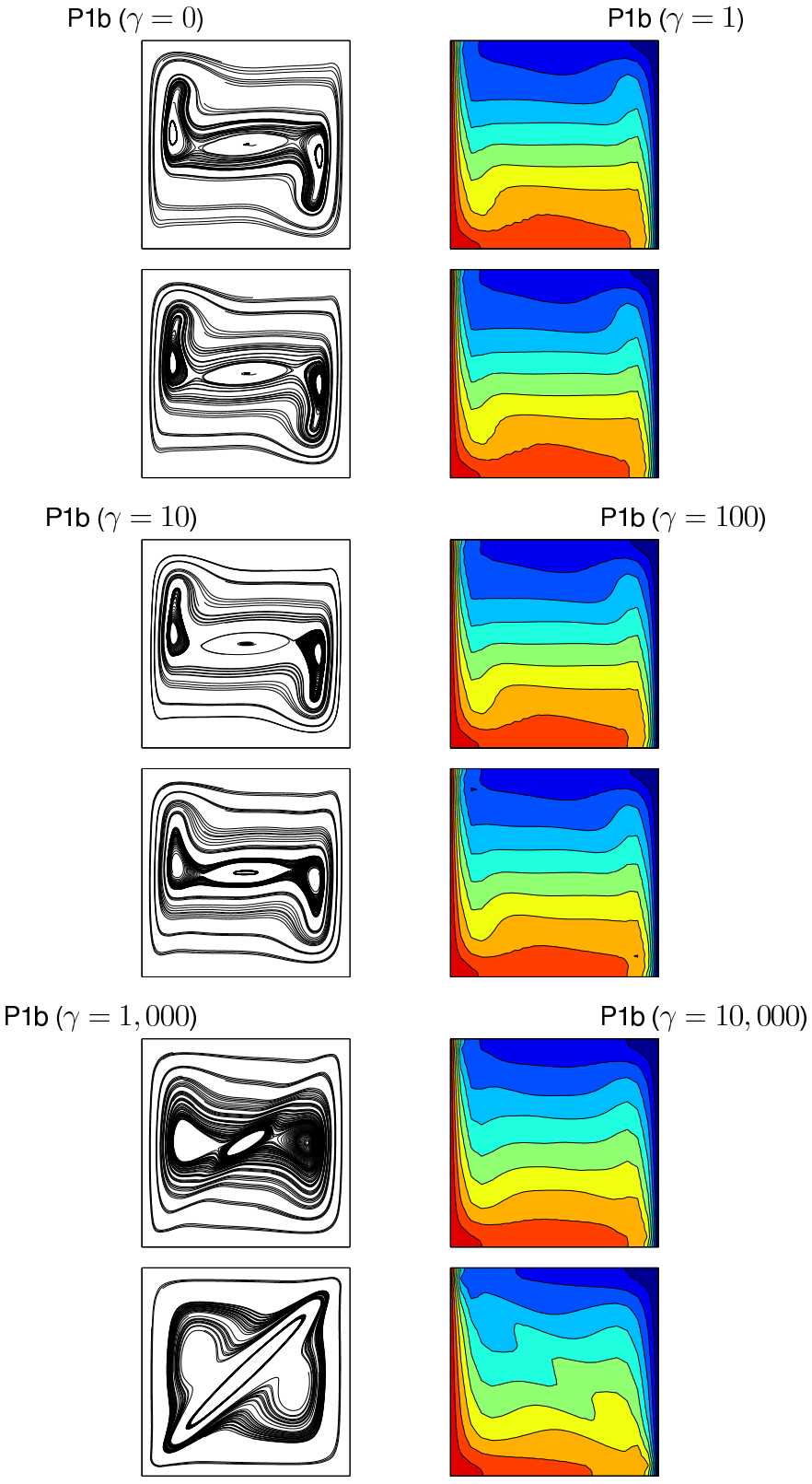

Figure 6: Solution plots of P1B with varying γ on the finer non-barycenter refined mesh for Pr=0.71

3.2 Comparison of solutions for natural convection in silicon oil (Pr=∞)

We now consider the same test problem, but for natural convection in silicon oil instead of air. Here, $Pr = \infty$, and so the NSE momentum equation reduces to the Stokes equation. Thus, here, the NSE nonlinearity is not playing a role in creating instability. The same meshes and algorithms are used as in the above test problem, and again we take $Ra = 10^6$.

We first compute a reference solution on the fine mesh, and display the solution's velocity and temperature in Figure 7.

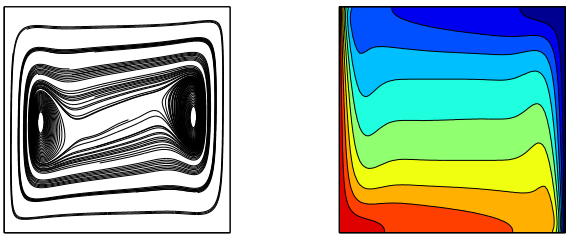

Figure 7: The velocity streamlines, and temperature contours of the reference solution for Pr=∞ and Ra=10^6.

Results on the coarser meshes are shown as velocity streamlines and temperature contours in Figures 8-10, and divergence errors are shown in Table 2. The divergence errors are as expected, with SV providing much better mass conservation than the other methods, and the other methods' mass conservation improving as γ increases.

Figure 8 shows results of the Pr=∞ computations on the barycenter refined mesh for SV, TH and P2P0 with varying γ. Here, SV finds a good solution that matches the reference solution, while finding good solutions for both TH and P2P0 requires heavy grad-div stabilization. Figure 9 shows results of computations on the non-barycenter refined mesh for TH and P2P0 with varying γ. We observe similar results as those on the barycenter refined mesh, in that both TH and P2P0 need heavy grad-div stabilization to find good solutions. For the P1B results in Figure 10, we observe that with small γ, the velocity streamlines and temperature contours are inaccurate compared to the reference solution when $\gamma = 0$. As γ increases to 100, some improvement in the velocity streamlines is observed, but just as in the Pr=0.71 case, further increasing γ destroys the solution.

4 Conclusions

We have provided theory and numerical experiments that suggest when there is a large forcing in the momentum equation, and when the irrotational part of the forcing is large relative to the divergence-free part, large stabilization parameters are necessary if grad-div stabilization is used with mixed finite elements. This was verified for two test problems where such phenomena arise, which validated our theory. Here, we saw with the TH and P2P0 element choices that heavy grad-div stabilization was necessary. Note that P2P0 elements conserve mass locally, which reveals that local mass conservation may also not be sufficient for such problems. For low order elements such as P1B, stabilization of the divergence error is necessary, but grad-div stabilization can 'over-stabilize' and destroy the so-

element	mesh	γ	$\|\nabla \cdot u_h\|$
SV	barycenter	0	1.46457e-7
P2P0	barycenter	0	(Newton failed)
P2P0	barycenter	1	(Newton failed)
P2P0	barycenter	10	561.362
P2P0	barycenter	100	100.167
P2P0	barycenter	1k	10.647
P2P0	barycenter	10k	1.07046
TH	barycenter	0	322.845
TH	barycenter	1	199.753
TH	barycenter	10	59.8523
TH	barycenter	100	8.53961
TH	barycenter	1,000	0.89697
TH	barycenter	10,000	0.0901575
P2P0	coarser non-bary	0	1915.31
P2P0	coarser non-bary	1	1413.69
P2P0	coarser non-bary	10	550.21
P2P0	coarser non-bary	100	82.5121
P2P0	coarser non-bary	1,000	8.59894
P2P0	coarser non-bary	10,000	0.863363
TH	coarser non-bary	0	78.3519
TH	coarser non-bary	1	51.8061
TH	coarser non-bary	10	21.1296
TH	coarser non-bary	100	4.36193
TH	coarser non-bary	1,000	0.529689
TH	coarser non-bary	10,000	0.0546587
(P1b,P1)	finer non-bary	0	285.469
(P1b,P1)	finer non-bary	1	193.811
(P1b,P1)	finer non-bary	10	77.838
(P1b,P1)	finer non-bary	100	42.993
(P1b,P1)	finer non-bary	1,000	28.076
(P1b,P1)	finer non-bary	10,000	9.321

Table 2: Mass conservation of the different solutions for Ra=10^6 and Pr = ∞.

lution. A good alternative for these problems is to use divergence-free mixed finite elements, such as Scott-Vogelius.

References

[1] G. Barakos, E. Mitsoulis, and D. Assimacopoulos. Natural convection flow in a square cavity revisited: laminar and turbulent models with wall functions. *Int. J. Numer. Methods Fluids*, 18:695–719, 1994.

[2] M. Braack, E. Burman, V. John, and G. Lube. Stabilized finite element methods for the generalized Oseen problem. *Comp. Meth. Appl. Mech. Engrg.*, 196(4–6):853–866, 2007.

[3] S. Brenner and L.R. Scott. *The Mathematical Theory of Finite Element Methods*. Springer-Verlag, 1994.

[4] F. Brezzi and M. Fortin. *Mixed and Hybrid Finite Elements*, volume 15 of *Springer Series in Computational Mathematics*. Springer, 1991.

[5] M. Case, V. Ervin, A. Linke, and L. Rebholz. A connection between Scott-Vogelius elements and grad-div stabilization. *SIAM Journal on Numerical Analysis*, 49(4):1461–1481, 2011.

[6] S. Chippada, C. Dawson, M. Martinez, and M. Wheeler. A projection method for constructing a mass conservative velocity field. *Computational Methods in Applied Mechanics and Engineering*, 157:1–10, 1998.

[7] A. Cibik and S. Kaya. A projection-based stabilized finite element method for steady state natural convection problem. *Journal of Mathematical Analysis and Applications*, 381:469–484, 2011.

[8] D. de Vahl Davis. Natural convection of air in a square cavity: A benchmark solution. *Int. J. Numer. Methods Fluids*, 3:249Ð264, 1983.

[9] H. Elman, D. Silvester, and A. Wathen. *Finite Elements and Fast Iterative Solvers with applications in incompressible fluid dynamics*. Numerical Mathematics and Scientific Computation. Oxford University Press, Oxford, 2005.

[10] S. Ganesan and V. John. Pressure separation — a technique for improving the velocity error in finite element discretisations of the Navier-Stokes equations. *Appl. Math. Comp.*, 165(2):275–290, 2005.

[11] V. Girault and P.-A. Raviart. *Finite Element Methods for Navier-Stokes Equations*, volume 5 of *Springer Series in Computational Mathematics*. Springer-Verlag, Berlin, 1986.

[12] W. Layton. *An Introduction to the Numerical Analysis of Viscous Incompressible Flows*. SIAM, 2008.

[13] W. Layton, C. Manica, M. Neda, M.A. Olshanskii, and L. Rebholz. On the accuracy of the rotation form in simulations of the Navier-Stokes equations. *Journal of Computational Physics*, 228(9):3433–3447, 2009.

[14] A. Linke. *Divergence-free mixed finite elements for the incompressible Navier-Stokes Equation*. PhD thesis, University of Erlangen, 2008.

[15] A. Linke, L. Rebholz, and N. Wilson. On the convergence rate of grad-div stabilized Taylor-Hood to Scott-Vogelius solutions for incompressible flow problems. *Journal of Mathematical Analysis and Applications*, 381:612–626, 2011.

[16] M. Wheeler M. Guillot, B. RiviŔre. Discontinuous galerkin methods for mass conservation equations for environmental modeling. In W. G. Gray S. M. Hassanizadeh, R. J. Schotting and G. F. Pinder, editors, *Developments in Water Science, Computational Methods in Water Resources*, pages 947–955, 2002.

[17] C. Manica, M. Neda, M.A. Olshanskii, and L. Rebholz. Enabling accuracy of Navier-Stokes-alpha through deconvolution and enhanced stability. *M2AN: Mathematical Modelling and Numerical Analysis*, 45:277–308, 2011.

[18] M.A. Olshanskii and A. Reusken. Grad-Div stabilization for the Stokes equations. *Math. Comp.*, 73:1699–1718, 2004.

[19] Maxim Olshanskii, Gert Lube, Timo Heister, and Johannes Löwe. Grad-div stabilization and subgrid pressure models for the incompressible Navier-Stokes equations. *Comput. Methods Appl. Mech. Engrg.*, 198(49-52):3975–3988, 2009.

[20] J. Qin. *On the convergence of some low order mixed finite elements for incompressible fluids*. PhD thesis, Pennsylvania State University, 1994.

[21] H.-G. Roos, M. Stynes, and L. Tobiska. *Robust numerical methods for singularly perturbed differential equations*, volume 24 of *Springer Series in Computational Mathematics*. Springer, Berlin, 2nd edition, 2008.

SV

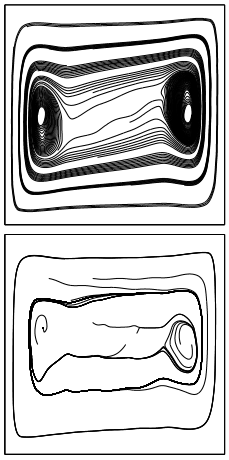

TH ($\gamma = 0$)

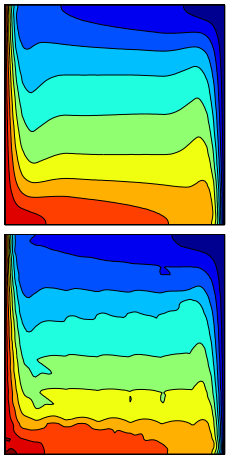

TH ($\gamma = 1$)

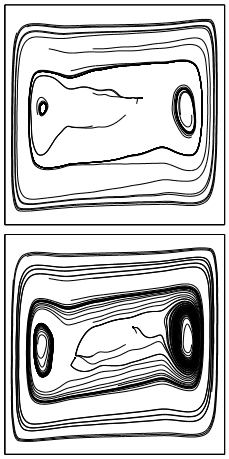

TH ($\gamma = 10$)

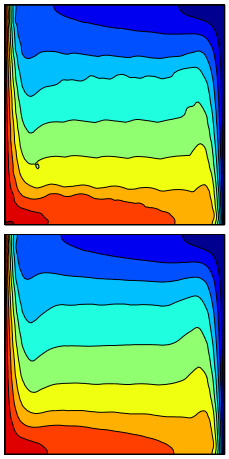

TH ($\gamma = 100$)

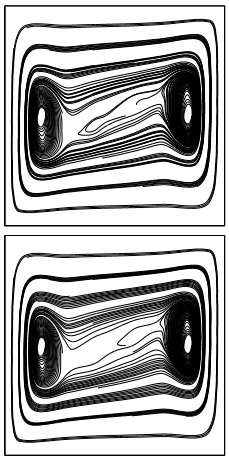

TH ($\gamma = 1,000$)

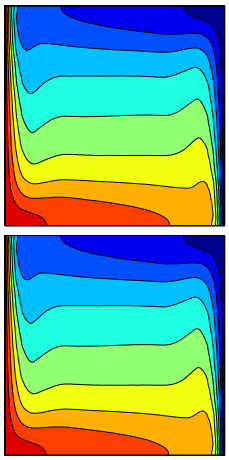

P2P0 ($\gamma = 0$) - Newton Failed

P2P0 ($\gamma = 100$)

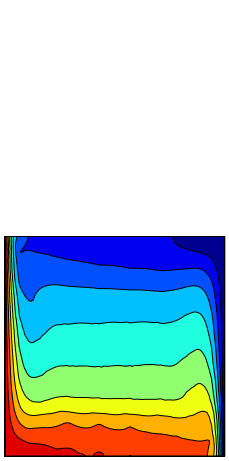

P2P0 ($\gamma = 1,000$)

P2P0 ($\gamma = 10,000$)

TH($\gamma = 0$)

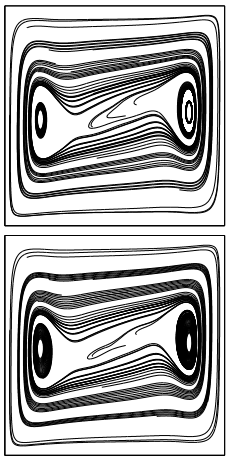

TH ($\gamma = 1$)

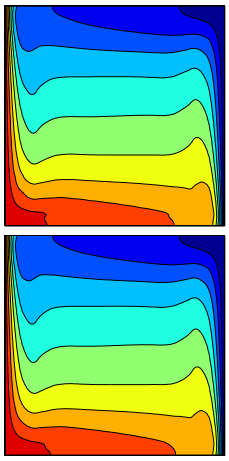

TH ($\gamma = 10$)

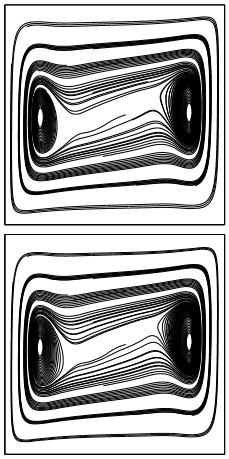

TH ($\gamma = 100$)

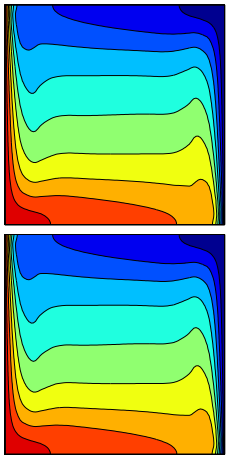

TH ($\gamma = 1,000$)

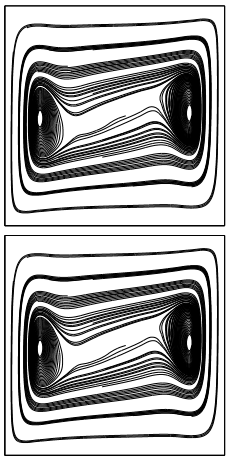

TH ($\gamma = 10,000$)

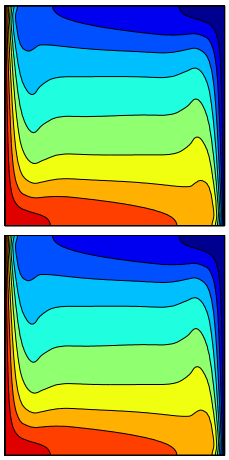

P2P0 ($\gamma = 0$)

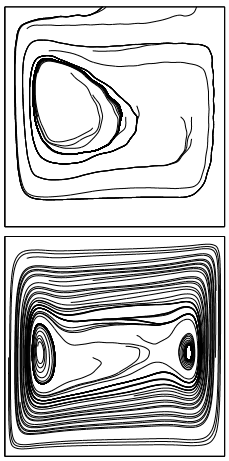

P2P0 ($\gamma = 100$)

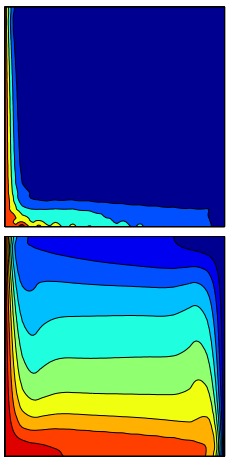

P2P0 ($\gamma = 1,000$)

P2P0 ($\gamma = 10,000$)

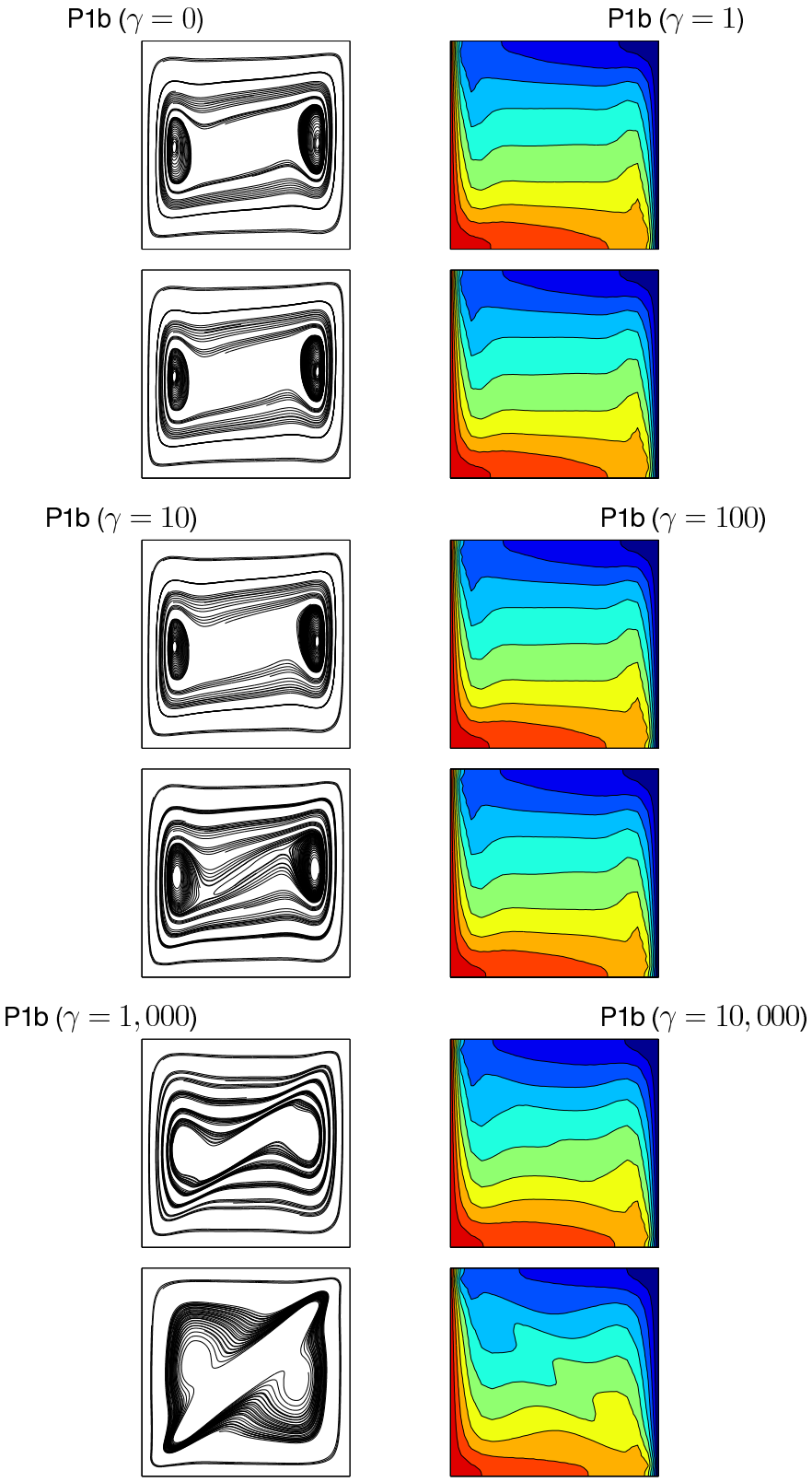

Figure 10: Solution plots of P1B with varying γ on the finer non-barycenter refined mesh for Pr=∞